SANDIA REPORT

SAND2018-14177
Unlimited Release
Printed December 2018

Evaluation of Secondary Gamma Environments at the Annular Core Research Reactor

Brian D. Hehr, Edward J. Parma, Gerald E. Naranjo

Prepared by
Sandia National Laboratories
Albuquerque, New Mexico 87185 and Livermore, California 94550

Sandia National Laboratories is a multimission laboratory managed and operated by National Technology and Engineering Solutions of Sandia, LLC, a wholly owned subsidiary of Honeywell International, Inc., for the U.S. Department of Energy's National Nuclear Security Administration under contract DE-NA0003525.

Issued by Sandia National Laboratories, operated for the United States Department of Energy by Sandia Corporation.

Available to DOE and DOE contractors from
U.S. Department of Energy
Office of Scientific and Technical Information
P.O. Box 62
Oak Ridge, TN 37831

Telephone: (865) 576-8401
Facsimile: (865) 576-5728
E-Mail: reports@osti.gov
Online ordering: http://www.osti.gov/scitech

Available to the public from
U.S. Department of Commerce
National Technical Information Service
5301 Shawnee Rd
Alexandria, VA 22312

Telephone: (800) 553-6847
Facsimile: (703) 605-6900
E-Mail: orders@ntis.gov
Online order: http://www.ntis.gov/search

SAND2018-14177
Unlimited Release
Printed December 2018

Evaluation of Secondary Gamma Environments at the Annular Core Research Reactor

Brian D. Hehr, Edward J. Parma, Gerald E. Naranjo
Applied Nuclear Technologies
Sandia National Laboratories
P.O. Box 5800
Albuquerque, New Mexico 87185-MS1146

Abstract

An overview of experimental and computational studies of prompt secondary gamma production and transport, executed under the auspices of the Readiness in Technical Base and Facilities (RTBF) program, is presented. Relevant experiments at the Annular Core Research Reactor (ACRR) were conducted in the FY2012 – FY2014 timeframe and pertain to the performance of various elemental calorimeters and the analytic fractionation of dose contributions to the calorimeter discs. In particular, the influence of the choice of prompt capture gamma production databases on the computed disc heating factors is discussed. Finally, the results of a polyurethane foam moderation experiment are detailed.

ACKNOWLEDGMENTS

ACRR experiments and related analyses were funded under the Readiness in Technical Base and Facilities (RTBF) program. The finalization of this SAND report was funded by the Radiation and Electrical Sciences (RES) program.

CONTENTS

FIGURES

TABLES

NOMENCLATURE

ACRR	Annular Core Research Reactor
C/E	Ratio of calculated and experimental values
CENDL	Chinese Evaluated Nuclear Data Library
ENDF	Evaluated Nuclear Data File
FWHM	Full width at half-max
JEFF	Joint Evaluated Fission and Fusion file
MCNP	Monte Carlo N-Particle (code)
RES	Radiation and Electrical Sciences
ROSFOND	Russian evaluated nuclear data library
RTBF	Readiness in Technical Base and Facilities
SNL	Sandia National Laboratories
TENDL	Talys-based Evaluated Nuclear Data Library
TTP	Time to Peak Pulse

1. INTRODUCTION

The production of secondary gammas from neutron reactions, principally the (n,γ) radiative capture reaction, can be a major contributor to the dose received by a component irradiated in a neutron or mixed neutron / gamma field. Details of secondary gamma production depend strongly on the elemental composition and geometric configuration characterizing the system of interest. For example, placing an element with a high capture cross section, such as cadmium, gold, or tantalum, in close proximity to the sensitive region of an electronic device can substantially enhance the dose to that region because of the small degree of geometric attenuation between the source and the target. In order to accurately quantify this effect, reliable data is needed for the energy spectrum and multiplicity of secondary gammas emitted per capture reaction. One purpose of the FY12 – FY14 calorimeter testing campaign at ACRR was to investigate the degree of alignment between experimental and calculated secondary capture gamma effects by conducting experiments sensitive to those effects, thereby probing published (n,γ) data libraries in an indirect manner.

A related phenomenon of import to secondary gamma production is the neutron moderating effect of materials surrounding sensitive components. One such material is polyurethane foam, which is commonly employed as potting material for electronic components or sub-systems. The presence of hydrogenous material in the vicinity of a sensitive component can substantially alter the displacement damage and total dose received by the component. Specifically, a higher degree of neutron moderation will generally reduce the amount of displacement damage (quantified, for example, via a 1-MeV equivalent neutron fluence) while possibly raising the total dose via enhanced capture gamma production. Therefore, validation of the spectral shift caused by the down-scattering material is helpful for asserting confidence in relevant modeling efforts.

2. RESULTS AND DISCUSSION

2.1. Calorimeter Experiments and Prompt Capture Data

The original series of calorimeter experiments, initiated in FY12, was devised with a twofold purpose in mind:

1) To explore novel calorimeter materials that may be well suited to particular applications
2) To verify that existing modeling capabilities are sufficient to capture the essential elements of the experimentally-observed responses, especially the component of calorimeter heating attributable to prompt (n,γ) capture reactions.

A comparison of the calculated vs. experimental heating factors of the original set of calorimeter disc elements (Si, Sn, Zr, Bi, W, Ta) was published in a paper [1] in FY14. One significant observation drawn from that work was the importance of using the MCNP *F8 tally in conjunction with electron transport in order to correctly compute the absorbed dose in the disc (rather than the kerma as would follow from an F4 or F6 tally). The improved agreement with experiment was particularly remarkable in the cadmium-wrapped experiment, in which the staggered, cylindrical array of calorimeters was surrounded by a sheet of cadmium of sufficient thickness so as to remove virtually all neutrons below the cadmium cutoff. Appendix A details the process of converting an MCNP F4, F6, or *F8 tally into the metric of disc heating per unit of reactor pulse energy.

Diagrams of the experimental setup pertinent to the FY14 paper are shown in Figure 2-1, and a schematic of the calorimeter internal structure is displayed in Figure 2-2. Differences among the F4, F6, and *F8 tallies under varying physics assumptions are explored concisely in Appendix B.

The calorimeter experiments also validated the potentially sizable impact of the prompt (n, γ) reaction contribution to calorimeter disc heating. Here, we are concerned with gamma rays that are born within the disc, either from slow neutron capture or from resonance absorption, and subsequently interact with the constituent atoms of the disc prior to escape. Intuitively, this contribution to heating might be expected to be rather small due to the minute dimensions of the disc (approximately 1 cm in diameter and 1 mm thick). In fact, the prompt "self" (n, γ) dose contribution can approach 50% or more of the total calorimeter response in a sufficiently well-thermalized neutron spectrum (as in the ACRR lead-polyethylene bucket) for certain high-Z calorimeter elements such as tungsten, tantalum, or gold that are simultaneously strong absorbers of low-energy neutrons and excellent attenuators of gamma rays. A quantitative comparison of the magnitudes of the various calorimeter heating contributions was discussed in [1]. Although the total heating factors derived from MCNP modeling, in conjunction with ENDF/B-VI or B-VII data, agreed well with experimental measurements among the set of six elements examined in that study, subsequent analyses of follow-on experiments have not yielded the same satisfactory agreement in indium or gold—two elements of interest in semiconductor device applications. This finding suggests that a more in-depth inquiry into the prompt (n, γ) capture data itself would be beneficial, in view of the fact that the accumulated validation evidence supported other aspects of the modelling approach. A summary of the measured and calculated disc heating factors is shown in Table 2-1.

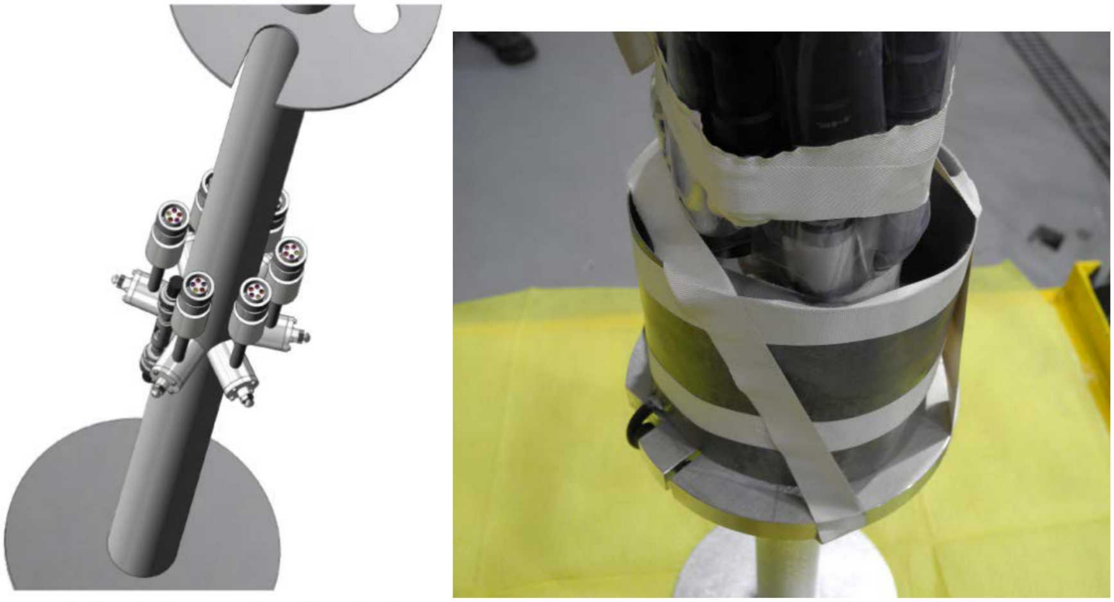

Figure 2-1. Schematic of calorimeter array on experimental pedestal (left panel) and photograph of tested, Cd-covered calorimeter array (right panel).

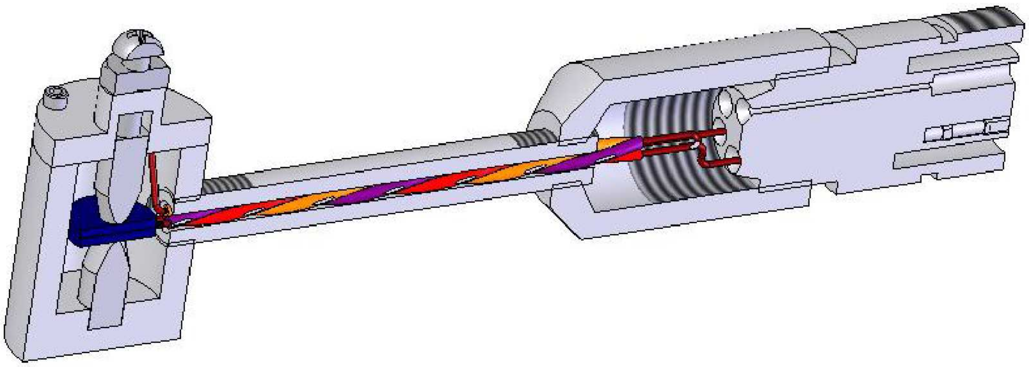

Figure 2-2. Diagram of calorimeter internals, showing thermocouple wires, disc material (dark blue), and disc mounting apparatus.

Much of the early ENDF gamma production data pertaining to the (n, γ) capture reaction originates from a 1970 Gulf General Atomic report [2], in which Ge(Li)-NaI spectrometer measurements of discrete and continuum gamma yields from 75 natural elements were condensed into binned spectra. Recently, R. B. Firestone of Lawrence Berkeley National Laboratory has spearheaded an endeavor to measure the neutron capture gamma ray cross sections of all naturally occurring elements, as well as select radioactive isotopes, at the Budapest reactor ([3],[4]). Their results, published in the form of an IAEA report [5], provide a high-resolution depiction of all discrete prompt gamma lines for elements of $Z \leq 19$ and of discrete lines in the low- and high-energy regimes for $Z \geq 20$. In the case of the higher-Z isotopes, the lines at intermediate energies are of sufficient density to constitute an effective continuum spectrum due to the large number of nuclear energy levels between the ground state and the initial excited state. This intermediate regime may be filled in via statistical model calculations using, e.g., the DICEBOX code [6] pending the acquisition of measured data of a higher resolution.

Figure 2-3 through Figure 2-6 show the continuous prompt capture gamma spectra of a few major elemental absorbers of interest, as extracted from various nuclear data compilations (specifically, from MF15 in ENDF-6-formatted compilations [7]). Also displayed on the plots are the discrete (EGAF) gamma production cross section data from the IAEA report [5]. All of the plotted probabilities correspond to an effective “zero neutron energy” condition in which the Q-value of the capture reaction far exceeds the kinetic energy of the incident neutron. If that condition is violated, then the gamma probability distribution will be altered accordingly. From the figures, it is apparent that localized spikes in the discrete cross sections tend to align with enhancements in the binned probabilities, though, as pointed out previously, there is generally a gap in the discrete data at intermediate energies. An additional observation is that gamma probability distributions from the TALYS-based Evaluated Nuclear Data Library (TENDL), which is derived analytically rather than experimentally, do not exhibit the isotope-specific localized structure evident in the other libraries.

Beyond the normalized probability distributions, radiation transport codes also require a multiplicity factor, defined as the number of photons emitted per neutron capture. This factor is specified as a function of neutron energy in MF12 of an ENDF-formatted library. As the incident neutron energy approaches zero, the multiplicity of (n,γ) capture gammas approaches a baseline quantity that is approximately equal to the reaction Q-value divided by the mean prompt gamma energy. At neutron energies on the order of the Q-value or larger, the photon multiplicity tends to be greater than the baseline value although the neutron capture cross section is typically vanishingly small at such energies in comparison to the cross sections characterizing competing channels such as elastic scattering, inelastic scattering, or knockout reactions.

Table 2-1. Experimental versus MCNP-computed heating factors, by element, using ENDF/B-VI or B-VII nuclear data and the full reactor model.

Disk type	EXPT. Heating (K / MJ)			CALC. Heating (K / MJ)		
	Bare	Cd-wrapped	Ratio (Cd:Bare)	Bare	Cd-wrapped	Ratio (Cd:Bare)
Si	0.081	0.167	2.1	0.075	0.158	2.1
Zr	0.198	0.408	2.1	0.185	0.407	2.2
Sn	0.248	0.501	2.0	0.228	0.510	2.2
Ta	0.970	1.270	1.3	1.002	1.244	1.2
W	0.878	1.252	1.4	0.806	1.222	1.5
Bi	0.648	1.378	2.1	0.654	1.402	2.1
Au	2.284			1.634		
Kovar	0.159			0.133		
In	1.010			0.630		
Cd	1.093			0.955		

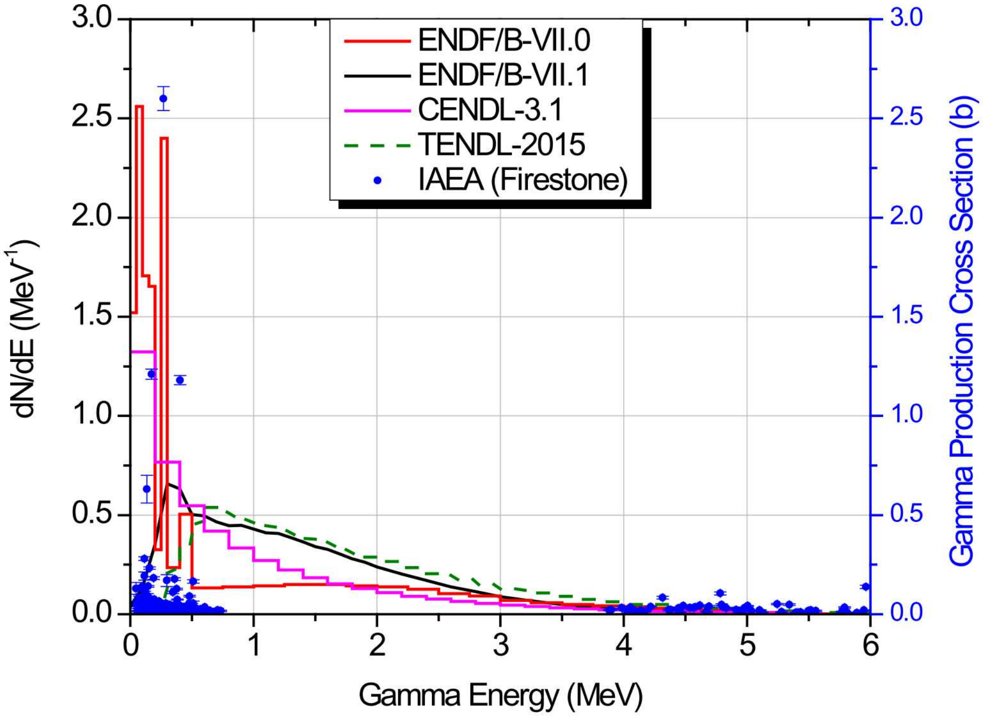

Figure 2-3. Neutron capture gamma spectrum for Ta-181 at $E_n \sim 0$.

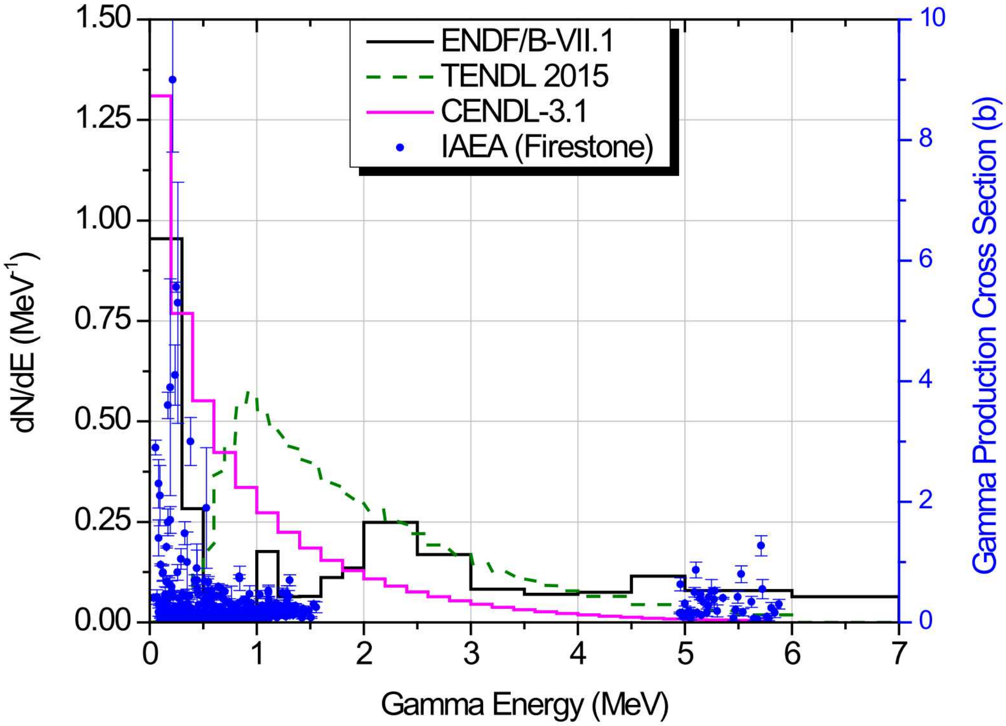

Figure 2-4. Neutron capture gamma spectrum for Au-197 at $E_n \sim 0$.

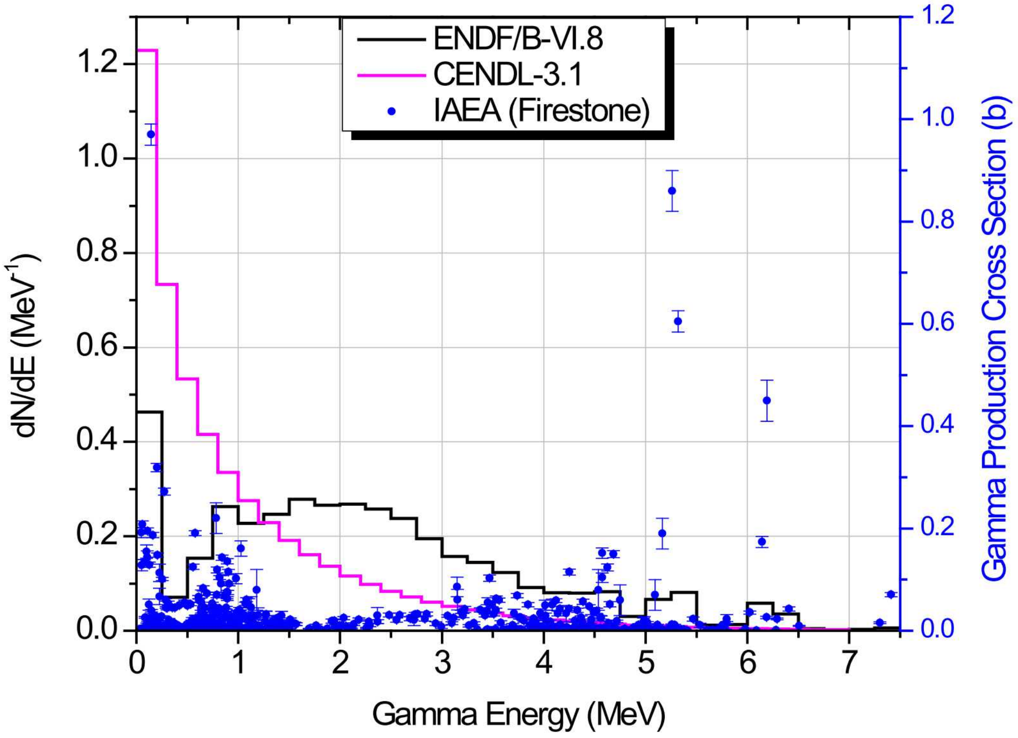

Figure 2-5. Neutron capture gamma spectrum for natural tungsten at $E_n \sim 0$.

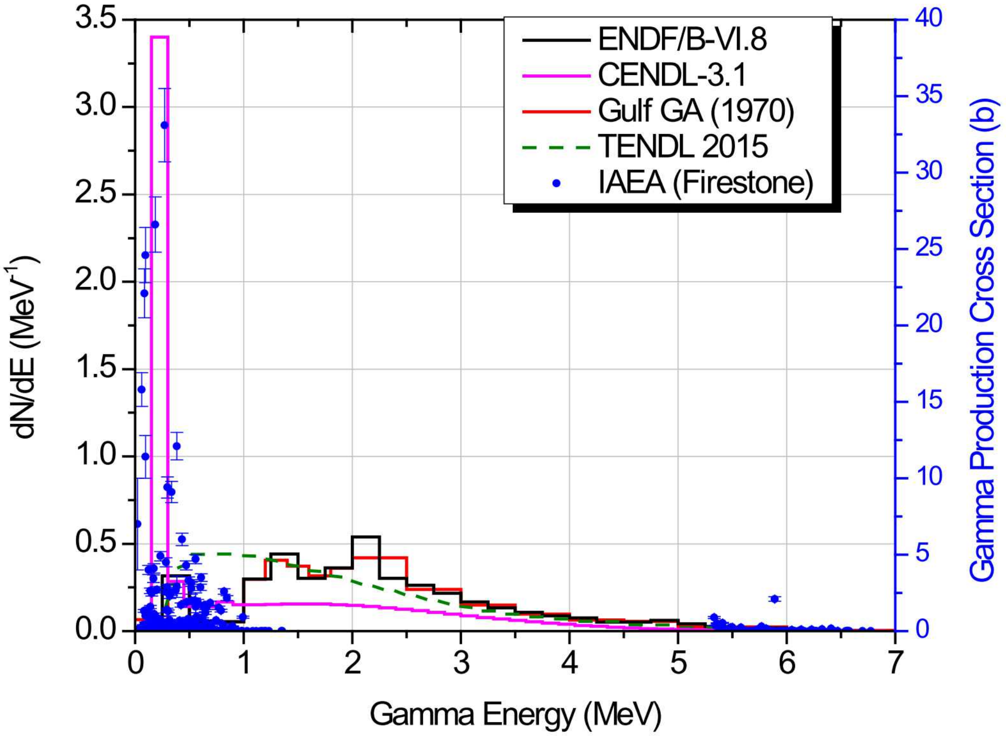

Figure 2-6. Neutron capture gamma spectrum for natural indium at E_n ~ 0.

In terms of the calorimeter response experiments, the practical effect of variations in the capture gamma spectra is to alter the mean heating efficiency of those gammas. This is illustrated in Figure 2-7, which shows MCNP-derived values of the energy deposited per source gamma as a function of gamma energy in two of the tested disc elements. For the purposes of these calculations, it was assumed that the gammas are created uniformly in the disc, which is approximately true if the self-shielding of low-energy neutrons is small.

At low gamma energies (i.e. tens to hundreds of keV), the generated gammas travel only a very short distance before being absorbed via the photoelectric effect and are, therefore, nearly 100% efficient in heating the disc, as is manifested in the plot by linear behavior with a slope approaching unity. Perfect efficiency is impossible, however, due to geometric edge effects. At intermediate energies (i.e. hundreds of keV up to about 1 MeV depending on the material), the efficiency drops off rapidly as the decreasing interaction cross section allows for a higher percentage of the gamma energy to escape the disc. At the upper end of the capture gamma spectrum, the decline in efficiency is partially offset by the advent and eventual dominance of the pair production reaction channel (particularly in higher-Z elements), though the offset is generally not sufficient to reverse the negative trend. The overall implication is that, under the constraint of a constant total quantity of gamma energy released per neutron absorption (i.e. the Q-value when E_n ~ 0), a shift in spectral content towards lower energies will result in a greater heating response. Thus, uncertainty in the gamma spectra—manifested, for example, as apparent variations among the data reported from different sources—would be expected to impact the computed calorimeter response significantly when the (n,γ) heating contribution is nontrivial.

The aforementioned spectral dependence of the response provides an impetus to investigate different evaluations of the (n,γ) production data in situations where the "default" ENDF-6-format libraries result in C/E discrepancies that cannot be attributed to other phenomena. From Table 2-1, it is seen that the largest deviations in C/E, percentage-wise, occur in indium and gold. In the case of indium, gamma production data is available from the ENDF/B-VI.8 library (for natural indium) and from the CENDL-3.1 library (for In-113 and In-115 separately). In the case of gold, gamma production data is reported in the ENDF/B-VII.1, JEFF-3.2, ROSFOND-2010, and CENDL-3.1 libraries; however, all of these originate from the same nuclear data evaluation for $E_n \sim 0$ with the exception of CENDL-3.1.

From Figure 2-4 and Figure 2-6, it is apparent that, for both materials, CENDL-3.1 exhibits more spectral content at low gamma energies as compared to the ENDF/B data. Coincidentally, the gamma heating efficiency in the disc (see Figure 2-7) is maximized at low gamma emission energies, so there is reason to expect a greater heating response under the CENDL-3.1 library. A breakdown of heating factor contributions versus cross section library is shown in Table 2-2 for tantalum, tungsten, gold, and indium—elements in which the disc (n,γ) heating component constitutes a large fraction of the total. For computational expediency, Table 2-2 was formulated using an isotropic surface source model in which individual calorimeters (as depicted in Figure 2-2) were bombarded with isotropic neutrons and gammas possessing a spectrum of energies equivalent to the actual environment at the ACRR testing position. In Table 2-3 and Table 2-4, the total heating factors derived from the surface source model and the full reactor model are compared, with the latter defined as the MCNP model of ACRR containing the full testing apparatus (see Figure 2-1).

Table 2-2, Table 2-3, and Table 2-4 show that MCNP calculations predict a substantial boost to the disc heating per MJ when the CENDL-3.1 gamma production data is employed, resulting in closer agreement with the experimentally-derived values for indium and gold. The exception to the observed trend is tantalum, for which similar heating factors ensue from the ENDF/B and CENDL data. Only the neutron data libraries associated with the calorimeter disc were modified in these calculations. Differences between ENDF/B and CENDL vis-à-vis the mean number of capture reactions per source neutron (see 3rd column of Table 2-2; *N(cap)*=number of (n,γ) capture reactions) are small compared to the differentials in the (n,γ) heating components of tungsten, gold, and indium; therefore, the gamma emission spectra are taken to be the reason for observed variations in the heating factor. This supposition is bolstered by the dominance of the capture gamma component of gamma production (see 4th column of Table 2-2; $N\gamma$=number of gammas produced), illustrating that the vast majority of gammas produced in all four disc materials arise from capture reactions (MT 102) as opposed to some other reaction mechanism.

The suggestion here is not that the CENDL emission spectra are superior to the ENDF/B spectra in a holistic sense, but rather that the CENDL spectra are such that better agreement is attained versus experiment when the spectra for indium and gold are folded with appropriate disc heating responses. While integral comparisons cannot provide conclusive validation evidence for the differential capture gamma spectrum, such metrics can constitute a useful benchmark (amongst a larger suite of evidence) against which a candidate spectrum may be tested.

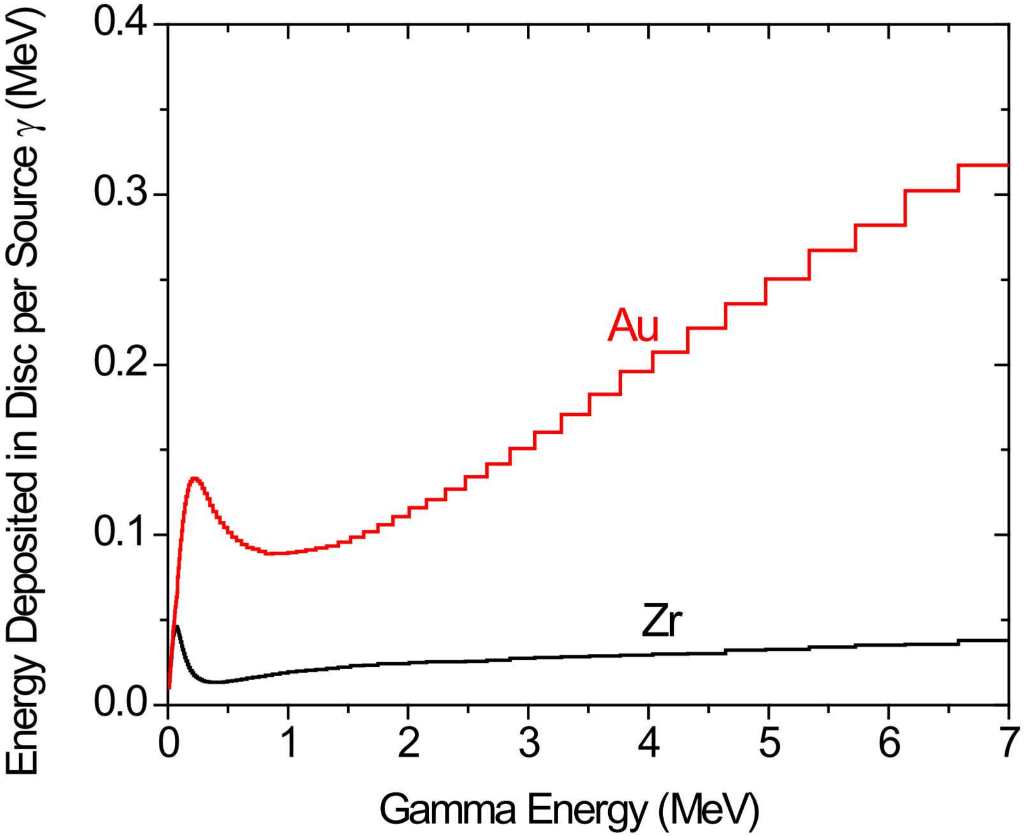

Figure 2-7. Mean energy deposited in calorimeter disc per source gamma, assuming a uniform volumetric source

Table 2-2. Computed heating factors and gamma production ratios in Ta, W, Au, and In using the isotropic surface source model.

Disc Type	Data Library	N(cap)ENDF / N(cap)CENDL	Nγ(cap) / Nγ(total)	CALC. Heating (K/MJ)			
				n	n/γ	γ	Total
Ta	ENDF/B-VII.0	1.035	0.986	0.018	0.484	0.405	0.907
	CENDL-3.1		0.984	0.02	0.493	0.405	0.918
W	ENDF/B-VII.0	0.951	0.913*	0.002	0.291	0.437	0.730
	CENDL-3.1		0.986	0.005	0.570	0.437	1.012
Au	ENDF/B-VII.0	1.000	0.990	0.001	0.983	0.473	1.458
	CENDL-3.1		0.996	0.006	1.659	0.473	2.138
In	ENDF/B-VI.0	1.003	0.998	0.002	0.360	0.185	0.547
	CENDL-3.1**		0.999	0.002	0.772	0.185	0.960

* ENDF/B-V.2 library for natural tungsten was employed to obtain this metric. Heating factors were evaluated using the ENDF/B-VII.0 isotopic libraries with appropriate abundances.

** In-115 library utilized; natural indium also contains a small fraction of In-113.

Table 2-3. Computed heating in gold disc: surface source versus full reactor model

Prompt γ Library	**CALC. Heating in Gold (K / MJ)**	
	Isotropic Surface Source	Full Reactor Model
ENDF/B-VII.1	1.458	1.634
CENDL-3.1	2.138	2.328

Table 2-4. Computed heating in indium disc: surface source versus full reactor model

Prompt γ Library	**CALC. Heating in Indium (K / MJ)**	
	Isotropic Surface Source	Full Reactor Model
ENDF/B-VI.8	0.547	0.63
CENDL-3.1	0.960	1.085

2.2. Polyurethane Foam Moderation Experiment

The filling of electronics sub-assemblies with potting foam is common practice to protect against adverse effects from shock or vibration and also to provide a barrier against the intrusion of reactive chemical agents. Such foam is typically comprised of an assortment of low-Z elements that normally includes a substantial fraction of hydrogen. Therefore, the foam acts as an effective moderator, altering the dose experienced at embedded components due to an external neutron source. A series of experiments were conducted at ACRR in 2014 to investigate the radiation response of a boral calorimeter embedded in a cylindrical piece of commercially-available, high-density polyurethane foam (see Figure 2-8), created by mixing a set of liquid precursors and curing the product. A combination of the lead-boron bucket and a boral calorimeter was chosen in order to ensure a sufficient degree of sensitivity to the change in the thermal neutron environment caused by the presence of the foam. The following table summarizes the relevant shots performed at ACRR.

Calorimeter Material	ACRR shot numbers	ACRR target energies
0.9 w/o Aluminum + 0.1 w/o Boron[nat.]	11088, 11089, 11090	50, 100, 150 MJ
0.955 w/o Aluminum + 0.045 w/o Boron [95% enriched in B-10]	11091, 11092, 11093	50, 100, 150 MJ

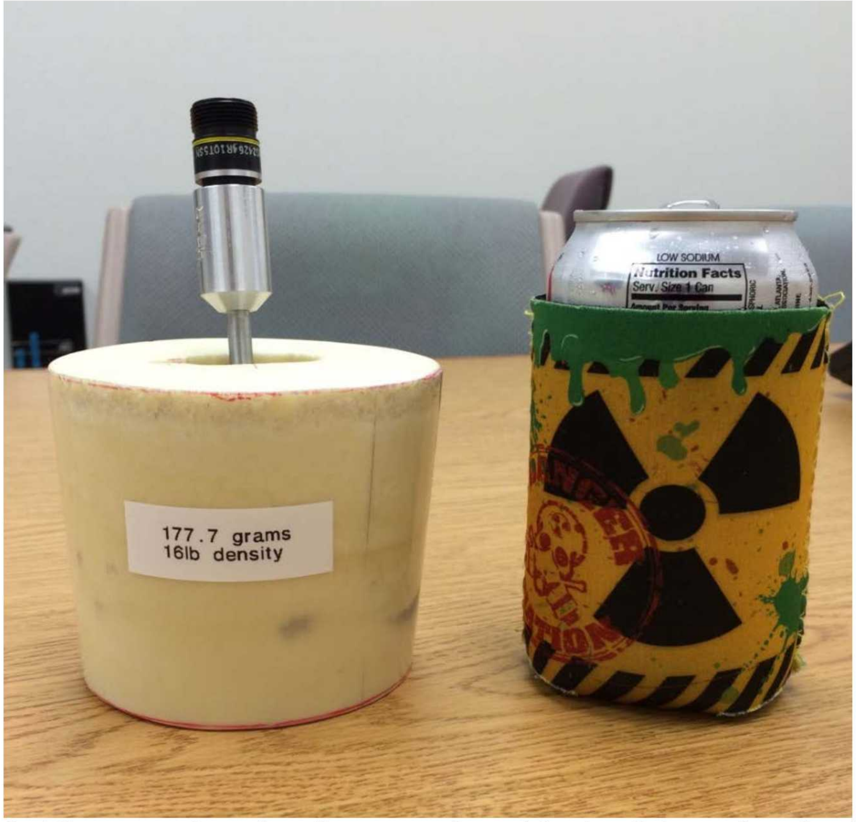

Figure 2-8. Diagram of moderation experiment test article—a boral calorimeter embedded in high-density foam. A 12-oz soda can is shown as a scale reference.

The time-dependent calorimeter voltage signals from shots 11088 – 11093 are shown in Figure 2-9 and Figure 2-10 below. To assess the heating response, the differential was taken between the voltage at (TTP + 3*FWHM) and the pre-shot voltage, where the quantity in parenthesis refers to the time to peak pulse plus three FHWM. These reference times were chosen to minimize error introduced into the heating response due to heat transfer from the calorimeter disc to other components of the calorimeter body. To address the noise in the signal, averaging windows were applied about both reference times. Specifically, the effective pre-shot signal was determined by averaging the calorimeter voltage from the time of first data acquisition until the pulse trigger time. Averaging about the (TTP + 3*FWHM) was somewhat more involved, as there are competing concerns—namely, to make the window large enough to effectively average out any oscillations in the signal, while also keeping the window small enough to avoid incorporating the signal ramp-down due to heat transfer. The window size, in this case, was selected based on Fourier analysis of the frequency components of the signal.

The Fourier frequency amplitude plot pertaining to shot 11088 is shown in Figure 2-11. There are two principal components of high-frequency noise, as indicated in the plot. The approach was to choose the window size such that the averaging window brackets two full oscillations of the lower-frequency noise component. Figure 2-12 shows the behavior of the signal over the time window fulfilling the aforementioned criterion for shot 11088; both components of noise are readily apparent in the figure.

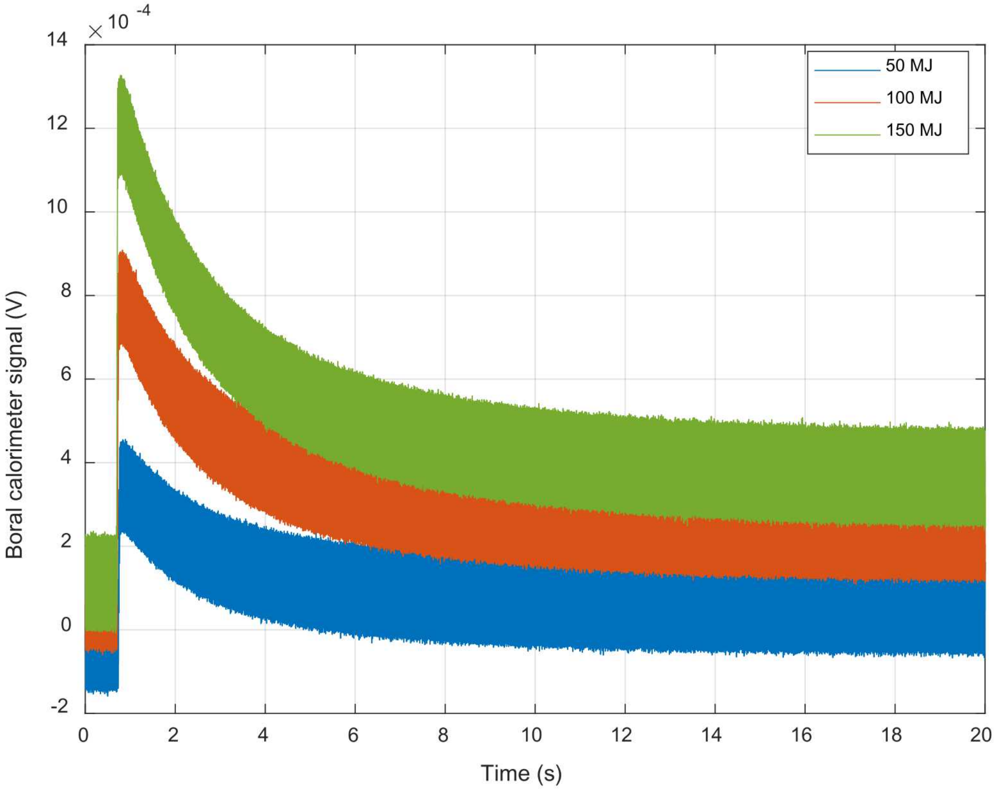

Figure 2-9. Response of Boral [10% B-nat] calorimeter to ACRR pulses

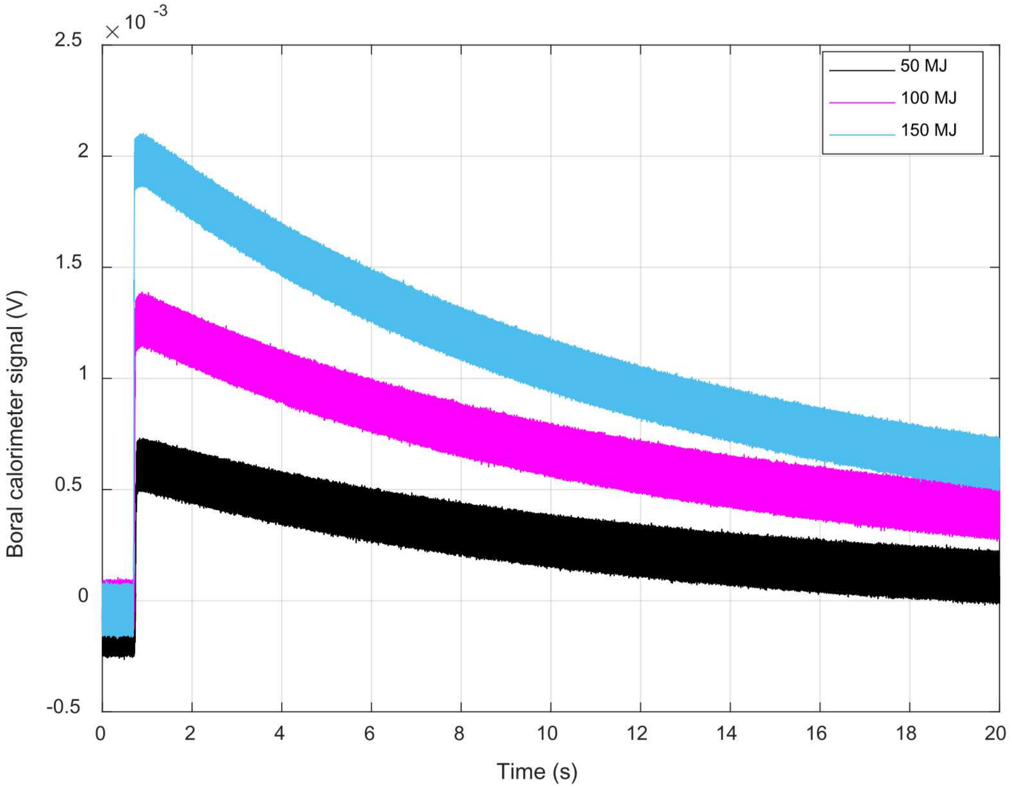

Figure 2-10. Response of Boral [4.5% B10-enriched] calorimeter to ACRR pulses

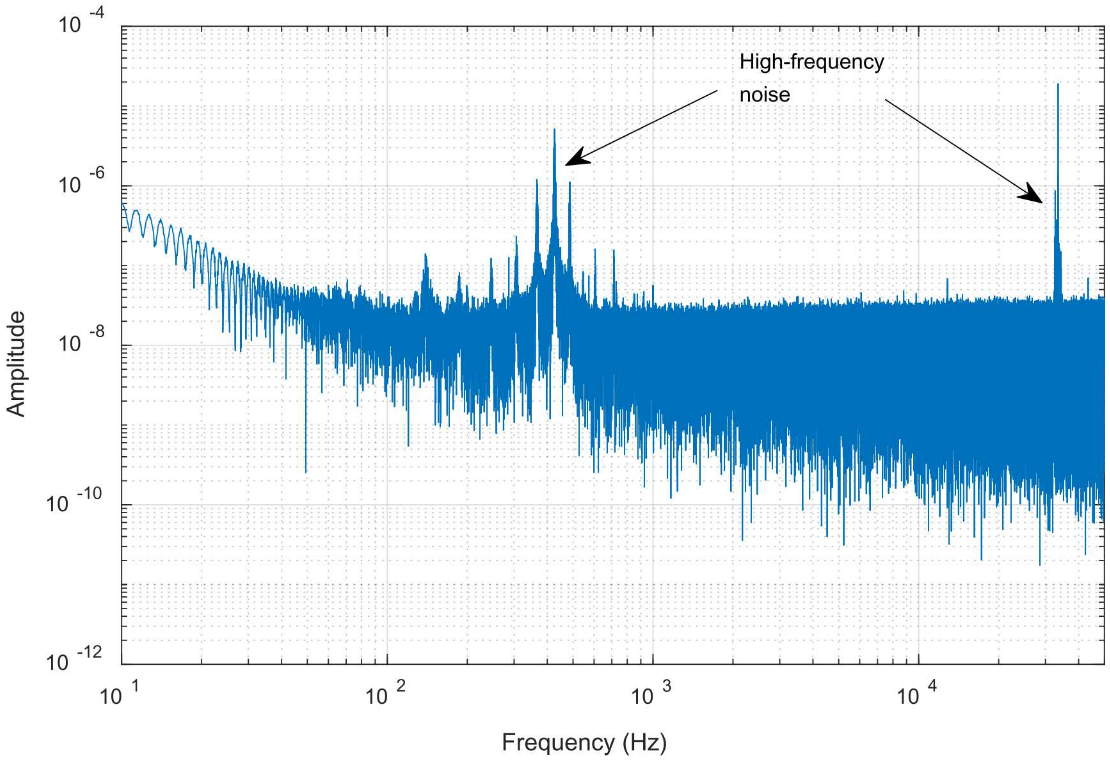

Figure 2-11. Frequency amplitude spectrum of boral calorimeter signal from shot 11088

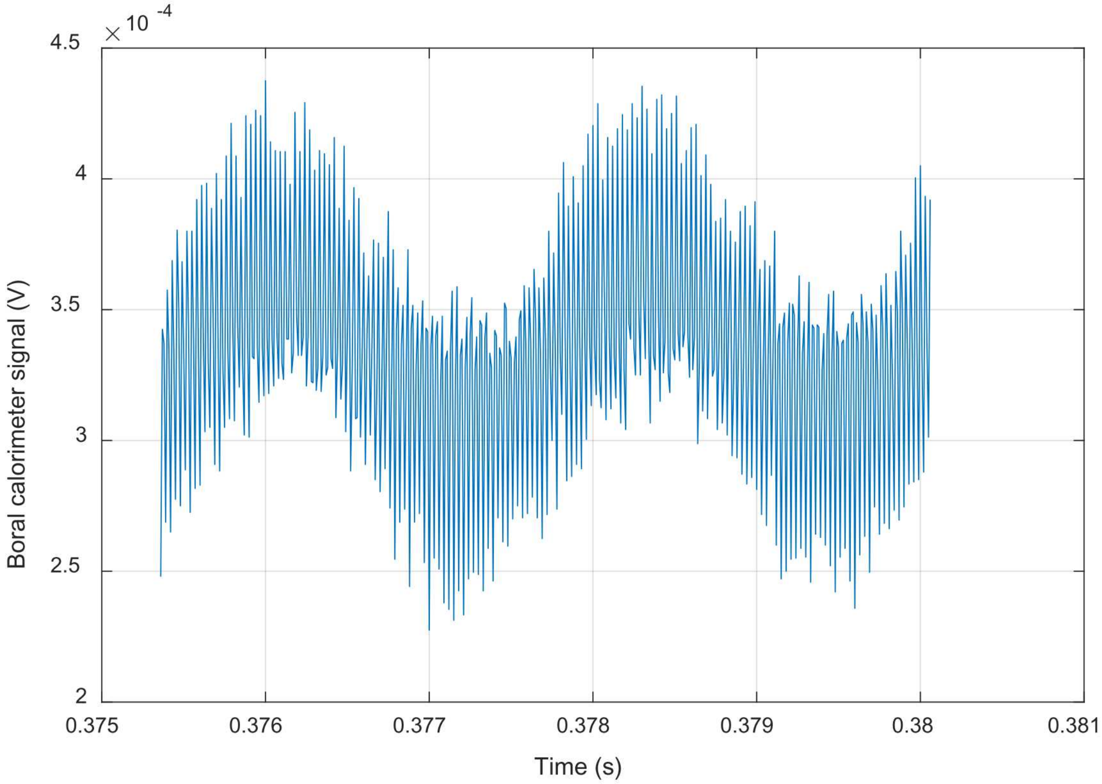

Figure 2-12. Boral calorimeter signal from shot 11088 plotted over the averaging window centered on (TTP + 3*FWHM)

Boral disc heating factors derived via the pre-shot to post-shot voltage differential are shown in Table 2-5 versus the targeted ACRR shot energy. Since the heating factors are normalized on a per MJ basis, it is anticipated that the response should be nearly constant as a function of shot energy. This is observed to be true at the two higher energies, but the lower shot energy yields a significantly different response. It is assumed that the values at higher energy are more accurate, as higher-shot energies bring about a larger signal-to-noise ratio in the calorimeter response. As expected, the heating response is larger in the enriched boron calorimeter due to the larger net number density of boron-10.

As a result of the favorable neutron moderation properties of hydrogen, the boral calorimeter response is quite sensitive to the elemental fraction of hydrogen in the surrounding foam. Attempts to obtain the elemental breakdown of the foam from the manufacturer were unsuccessful; however, representative breakdowns are available in the open literature, and the data acquired from ACRR experiments can be employed to discern a “best estimate” value for the hydrogen content. Figure 2-13 illustrates the calorimeter heating factor as a function of the atomic fraction of hydrogen in the foam, as computed using MCNP. For the purposes of this calculation, it was assumed that any variation in the hydrogen fraction was compensated for by an equal and opposite variation in the carbon content (i.e. to ensure that the sum of the atomic fractions remained equal to unity). Furthermore, it was assumed that variations introduced in the atomic fractions did not affect the aggregate mass density of the foam, which was a known, measured quantity.

It was found that the heating factor versus hydrogen fraction relationship could be represented accurately via the following equation:

$$HF = HF_o + A\exp\left[R\cdot(a/o)_H\right] \tag{2.1}$$

where HF is the heating factor, $(a/o)_H$ is the atomic fraction of hydrogen, and the remaining variables are fitted coefficients whose values are tabulated in Table 2-6.

Table 2-5. Boral heating versus shot target energy

Target Shot Energy (MJ)	Calc. Heating in Boral (K/MJ)	
	10 % B [nat.]	4.5% B [enr.]
50	0.128	0.213
100	0.154	0.256
150	0.158	0.255

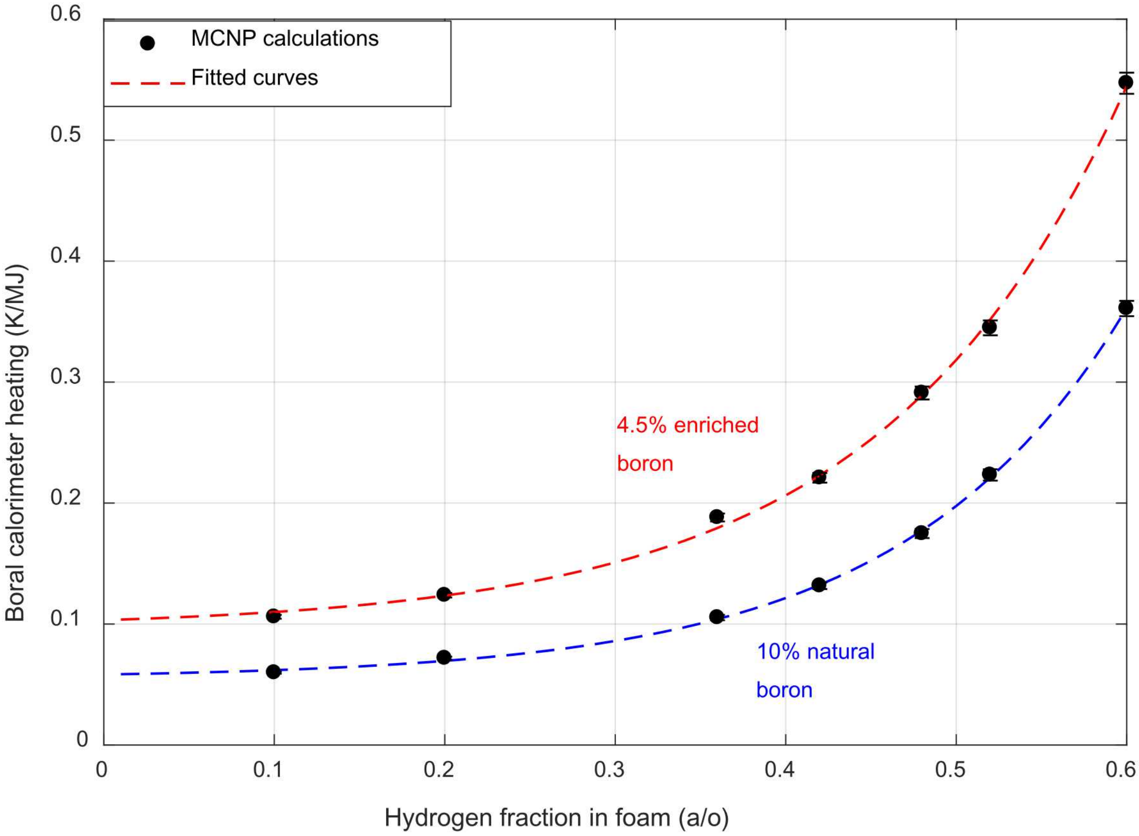

Figure 2-13. Boral response versus atomic number fraction of hydrogen in foam.

Table 2-6. Fitting parameters and uncertainties of dashed curves in Figure 2-13.

	10% natural boron		**4.5% enriched boron**	
Parameter	Value	Standard Error	Value	Standard Error
yo	0.05518	0.00224	0.09665	0.00625
A	0.00312	3.31571E-4	0.00658	0.00119
R	7.64191	0.17256	7.03436	0.29124

To obtain the "best estimate" values for the hydrogen fraction of the foam, equation (2.1) was employed in conjunction with heating factors from Table 2-5 (evaluated as the average of the 100 and 150 MJ values). The resulting fractions are 0.455 (a/o) from the natural boron dataset and 0.453 (a/o) from the enriched boron dataset. In comparison, hydrogen fractions found in literature are typically in the 0.5 – 0.6 (a/o) range ([9],[10]). The actual elemental content is sensitive to the specific manufacturing process utilized to create the foam precursor, and so the observed differences are not alarming.

3. CONCLUSIONS

The prompt gamma production characteristics of select elements have been investigated in the context of experimental calorimeter studies performed at ACRR in the FY12-FY14 timeframe. When irradiating in a highly neutron-moderating environment, the heating response of certain elemental calorimeters—generally those of relatively high atomic number possessing a large capture cross section—was shown to be sensitive to the database that is employed to represent the gamma production spectrum and multiplicity. It was found that the ENDF/B-VI or B-VII databases produced a good match between measured and calculated responses in silicon, zirconium, tin, tantalum, tungsten, bismuth, and cadmium. Responses in indium and gold exhibited a discrepancy that was largely resolved by instead utilizing the CENDL-3.1 databases. This observation, however, is not a conclusive indictor of superiority of the CENDL database vis-à-vis capture gamma spectra and multiplicities in indium and gold, since the metric under consideration is an integral, spectrum-folded quantity that may obscure "compensating defects" in the microscopic data.

As expected, the moderation properties of a foam encapsulate (used, for example, in electronics potting) are strongly dependent on its hydrogen content, which is subject to some degree of variability based on manufacturing and curing processes. An estimate of the hydrogen content of a specimen of cured foam was inferred by comparing fitted, MCNP-derived response curves against the measured response of an embedded boral calorimeter under varying conditions at ACRR. The resulting atomic fraction of hydrogen (~0.45) was found to accord well with representative estimates obtained from literature.

4. REFERENCES

[1] B. D. Hehr, E. J. Parma, C. D. Peters, G. E. Naranjo, and S. M. Luker. *Eur. Phys. J. WoC*, **106**, 01001, (2016).

[2] V. J. Orphan, N. C. Rasmussen and T. L. Harper. "Line and Continuum Gamma-Ray Yields from Thermal-Neutron Capture in 75 Elements", Gulf General Atomic Inc., Technical Report GA-10248, (1970).

[3] R. B. Firestone et al., *AIP Conf. Proc.*, **769**, 219, (2005).

[4] R. B. Firestone et al., *Nucl. Data Sheets*. **119**, 79, (2014).

[5] R. B. Firestone et al., "Database of Prompt Gamma Rays from Slow Neutron Capture for Elemental Analysis", IAEA STI/PUB/1263, 251, (2007).

[6] F. Bečvář, *Nucl. Instr. Meth. A*, **417**, 434, (1998).

[7] Cross Section Evaluation Working Group, "ENDF-6 Formats Manual," Report BNL-90365-2009 Rev. 1, M. Herman and A Trkov, Ed., (2010).

[8] M. Angelone, P. Batistoni, R. Bedogni, M. Chiti, A. Gentile, A. Esposito, M. Pillon and R. Villari, *Radiation Measurements*, **46**, 1737 (2011).

[9] M. W. Gregson, P. J. Griffin, P. J. Cooper, D. Vortolomei, E. R. Sanchez, J. A. Doorn, C. D. Peters and S. J. Manson. "Lessons Learned from Neutron Gamma Analysis of High Fidelity Complex Geometry Models," Hardened Electronics and Radiation Technologies (HEART) conference, Tucson, Arizona, Apr. 19 – 23, (2010).

[10] *Toxicology, Survival and Health Hazards of Combustion Products*, edited by David Purser, Robert Maynard, and James Wakefield, The Royal Society of Chemistry, 2016, p. 59.

APPENDIX A: CONVERSION FROM MCNP TALLIES TO RAD/MJ AND ΔT/MJ IN REACTOR

Prior to the application of multipliers, the MCNP F4 tally is in units of:

$$\left(\frac{fluence}{source-n}\right)=\left(\frac{1}{cm^2\cdot source-n}\right)$$

The FM cards are of the form:

FM4 C MAT_NUMBER -5 -6 [photons]
FM4 C MAT_NUMBER -4 1 [neutrons]

where the last two numbers in each FM card are the "reaction numbers", denoting energy-dependent fluence multipliers. The objective is to compute (rad/MJ) or (K/MJ). First, to get energy deposition per unit volume per source neutron:

$$\left(\frac{1}{cm^2\cdot source-n}\right)\cdot\left(\overbrace{b\cdot\frac{MeV}{collision}}^{\text{reaction numbers}}\right)\cdot\left(\frac{10^{-24}cm^2}{b}\right)\left(\frac{\rho N_A}{M}\right)\ \rightarrow\ \left[\frac{MeV}{cm^3\cdot source-n}\right]$$

in which ρ is the mass density, N_A is Avogadro's number, M is the effective atomic mass number, and the two reaction numbers are chosen to correspond to total microscopic cross section and mean energy deposited per collision respectively. Next, to get (rad/source-n):

$$\left(\frac{MeV}{cm^3\cdot source-n}\right)\left(\frac{rad}{0.01\ J/kg}\right)\left(\frac{1}{\rho}\right)\left(\frac{1000g}{kg}\right)\left(\frac{1.6E-13\ J}{MeV}\right)\ \rightarrow\ \left[\frac{rad}{source-n}\right]$$

In the case of the F6 tally, the tally units are energy deposited (in MeV) per gram per source particle, and so the conversion is:

$$\left(\frac{MeV}{g\cdot source-n}\right)\left(\frac{rad}{0.01\ J/kg}\right)\left(\frac{1000g}{kg}\right)\left(\frac{1.6E-13\ J}{MeV}\right)\ \rightarrow\ \left[\frac{rad}{source-n}\right]$$

In the case of the *F8 tally, the tally units are energy deposited (in MeV) per source particle, and so the conversion is:

$$\left(\frac{MeV}{source-n}\right)\left(\frac{1}{tally\_mass}\right)\left(\frac{rad}{0.01\ J/kg}\right)\left(\frac{1000g}{kg}\right)\left(\frac{1.6E-13\ J}{MeV}\right)\ \rightarrow\ \left[\frac{rad}{source-n}\right]$$

Then, to get (rad/MJ):

$$\left(\frac{rad}{source-n}\right)\left(\frac{2.4\ source-n}{fission}\right)\left(\frac{fission}{180\ MeV}\right)\left(\frac{1MeV}{1.6E-19\ MJ}\right)\ \rightarrow \left[\frac{rad}{MJ}\right]$$

which assumes a localized energy deposition of 180 MeV per fission event as well as an average neutron production of 2.4 per thermal neutron-induced fission in U-235. Finally, the adiabatic heating per MJ may be obtained from the (rad/MJ) figure via:

$$\left(\frac{rad}{MJ}\right)\left(\frac{0.01\ J/kg}{rad}\right)\left(\frac{kg}{1000g}\right)\left(\frac{1}{C_P}\right)\ \rightarrow \left(\frac{K}{MJ}\right)$$

where C_P is the heat capacity in units of J/(g·K).

APPENDIX B: CONVERGENCE OF F4, F6, AND *F8 TALLIES

Convergence among the F4, F6, and *F8 tallies was confirmed computationally by tallying the dose / kerma in an interior sub-region of a solid, cylindrical piece of tantalum. The tantalum test article is depicted in Figure B-1, with the tally cell (measuring 1.0 mm in height by 1.0 cm in diameter) identified. The thickness of the tantalum surrounding the tally region was then varied, and the dose was evaluated under four discrete energies of incident gamma rays, which were emitted such that the test article was exposed to an isotropic fluence of 7.22E+12 photons/cm^2. Electron transport was switched on for these calculations. The resulting kerma/dose versus equilibration layer thickness plots are shown in Figure B-2 through Figure B-5. In the context of this study, the equilibration layer thickness is defined as thickness of tantalum between the upper surface of the tally cell and the top surface of the test article, or, equivalently, the differential between the test article radius and the tally cell radius.

It was observed that if the thick-target bremsstrahlung approximation was turned on, the *F8 tally converged to the F6 tally while the F4 tally produced a larger value presumably because of the bremsstrahlung double counting issue discussed in [8]. In the absence of both electron transport and the thick target approximation, the F4 and F6 photon tallies become identical.

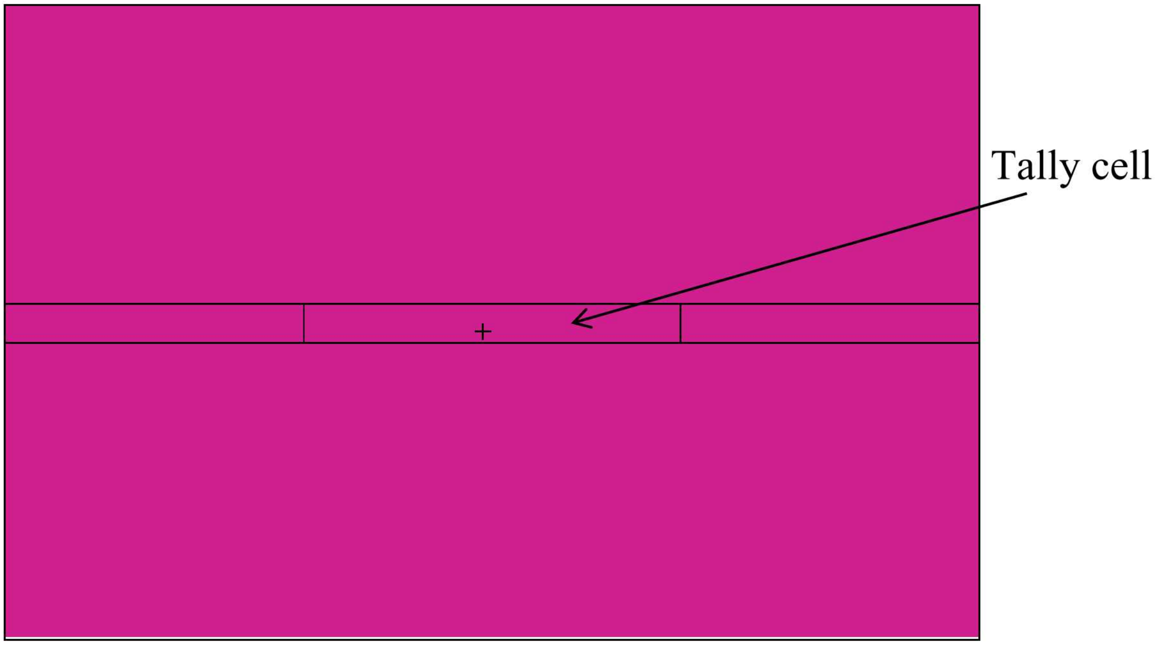

Figure B-1. Cross-sectional plot of cylindrical MCNP tally cell embedded inside a larger cylinder of tantalum.

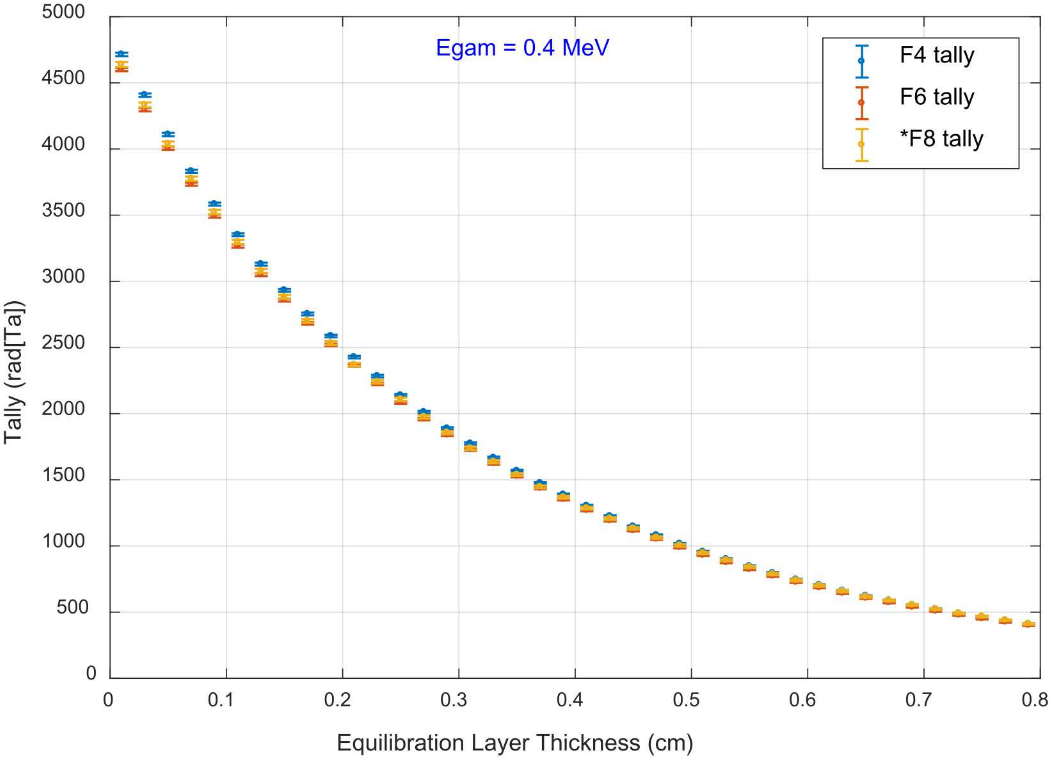

Figure B-2. Dose / kerma profile for the tantalum equilibration study with E_γ=0.4 MeV.

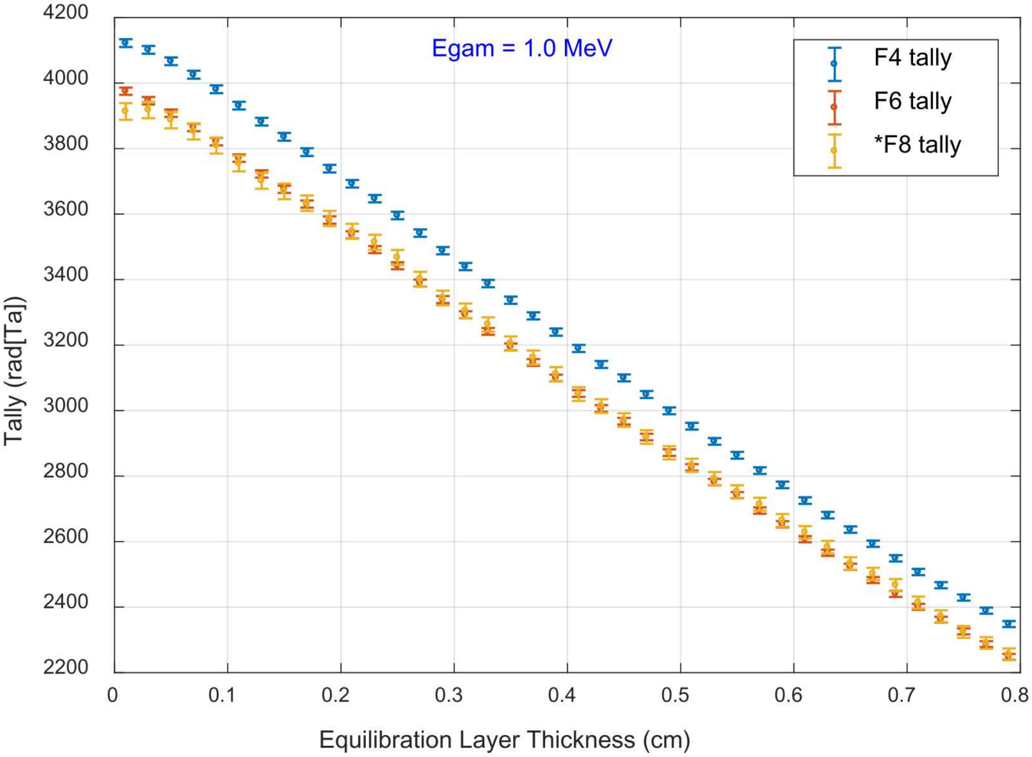

Figure B-3. Dose / kerma profile for the tantalum equilibration study with E_γ=1.0 MeV.

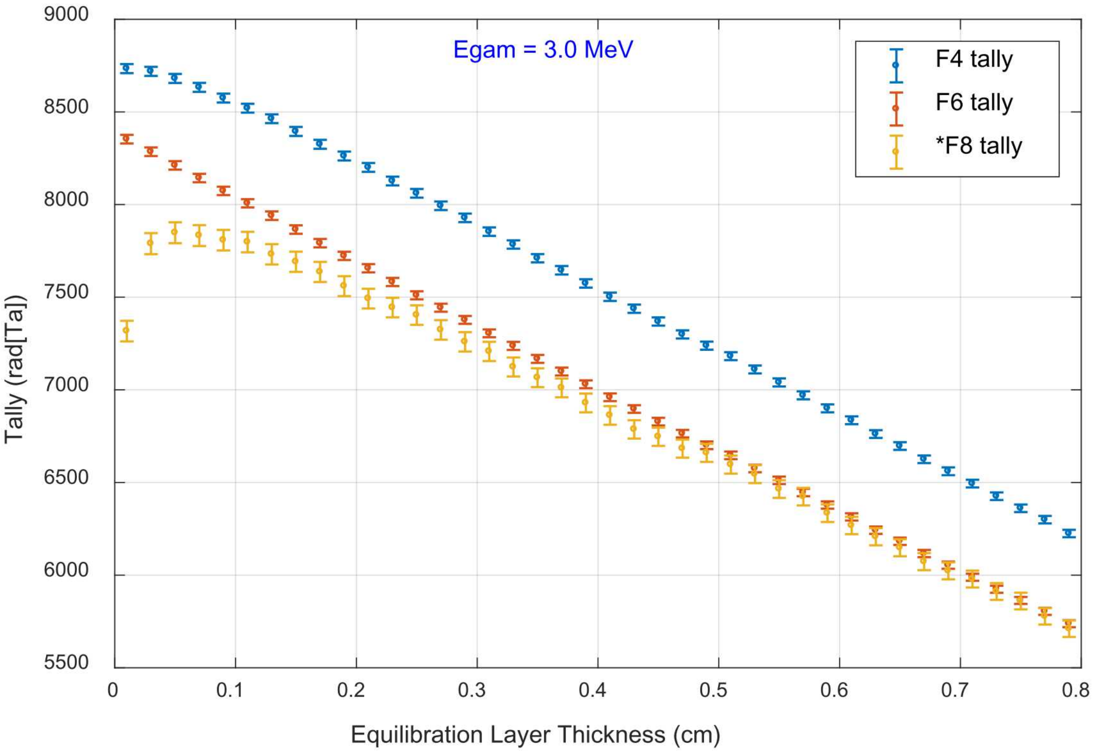

Figure B-4. Dose / kerma profile for the tantalum equilibration study with E_γ=3.0 MeV.

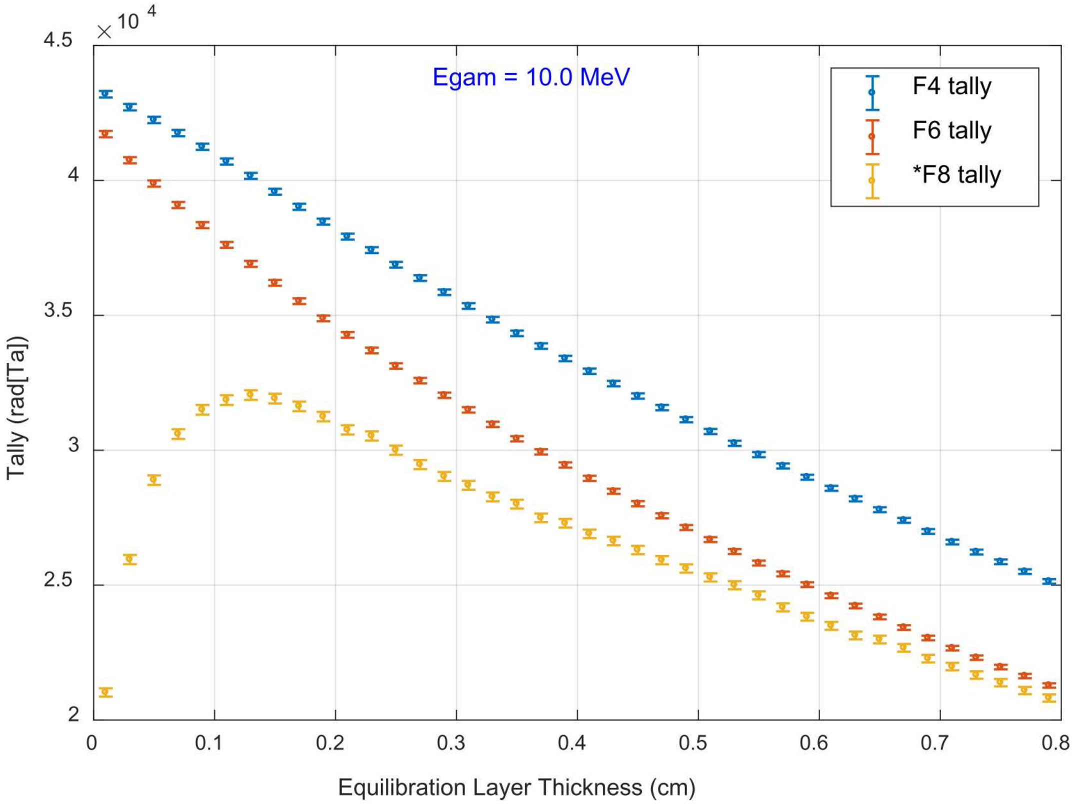

Figure B-5. Dose / kerma profile for the tantalum equilibration study with E_γ=10.0 MeV.

DISTRIBUTION

1	MS1056	William R. Wampler	1111
1	MS1146	Jamie E. Cash	1384
1	MS1146	Wu-Ching Cheng	1384
1	MS1146	Patrick J. Griffin	1300
1	MS1146	Edward J. Parma, Jr.	1383
1	MS1146	Kenneth O. Reil	1384
1	MS1179	Leonard Lorence	1341
1	MS0899	Technical Library	9536 (electronic copy)

Sandia National Laboratories